Effect of metal-oxide addition on the sintering of β-calcium orthophosphate

KIYOSHI ITATANI*, MIWA TAKAHASHI, F. SCOTT HOWELL, MAMORU AIZAWA
Department of Chemistry, Faculty of Science and Engineering, Sophia University, 7-1 Kioi-cho, Chiyoda-ku, Tokyo 102-8554, Japan
E-mail: itatani@sophia.ac.jp

The effect of metal-oxide addition (1 ∼ 10 mol %) on the sintering of β-calcium orthophosphate (β-$Ca_3(PO_4)_2$) was examined by pressureless sintering at 1070 °C for 5 h. The metal-oxide additives used were as follows: (i) monovalent metal-oxides, Li_2O, Na_2O, and K_2O; (ii) divalent metal-oxides, MgO, CaO, SrO, and BaO; (iii) trivalent metal-oxides, Al_2O_3 and Fe_2O_3; and (iv) tetravalent metal-oxides, SiO_2, TiO_2, and ZrO_2. The relative densities of the sintered β-$Ca_3(PO_4)_2$ compacts were reduced with increasing amounts of monovalent and divalent metal-oxide additions, except for the case of MgO addition when the relative density remained with increasing amount of MgO up to 4 mol %. In the case of trivalent metal-oxide additions, the relative density of sintered β-$Ca_3(PO_4)_2$ compact was reduced with increasing amount of Al_2O_3 addition, whereas it was enhanced with increasing amount of Fe_2O_3 addition and reached 98.7% at 10 mol % Fe_2O_3 addition. In the case of tetravalent metal-oxide additions, relative densities of the sintered β-$Ca_3(PO_4)_2$ compacts were slightly reduced with increasing amounts of SiO_2 and ZrO_2 additions, whereas no appreciable changes in the relative density were observed with increasing amount of TiO_2 addition.

1. Introduction

The calcium phosphates, e.g. calcium orthophosphate (β-$Ca_3(PO_4)_2$) and hydroxyapatite ($Ca_{10}(PO_4)_6(OH)_2$; HAp), are promising compounds for bone and tooth implant materials [1, 2]. In the case of HAp, porous ceramic is used as a bone substitute for biological fixation, whereas the dense ceramic works as space filler for bioactive fixation [2, 3]. The β-$Ca_3(PO_4)_2$ ceramic, which is usually utilized in the porous form, may also be expected to be permeated with cells and tissue and to be subsequently resorbed *in vivo* [3]. The porous β-$Ca_3(PO_4)_2$ ceramic that is placed in hard tissue functions is, therefore, regarded as a biodegradative scaffold for osteointegration [3]. The flexural strength of the dense β-$Ca_3(PO_4)_2$ ceramic is reported to be 138 MPa [4]; this value is slightly lower than that for dense human bones. The mechanical strength (e.g., flexural strength and fracture toughness) of the β-$Ca_3(PO_4)_2$ ceramic should not be degraded rapidly in order to utilize it as an implant material, although it ends up being replaced by bones.

Research on the properties of β-$Ca_3(PO_4)_2$ powder containing various kinds of metal oxides dates back to the 1950s, from the early attention to fertilizers [5]. Later, attention was directed toward the fabrication of the high strength β-$Ca_3(PO_4)_2$ ceramics with some metal oxides, e.g., zirconia (ZrO_2) [6], magnesia (MgO) [7], alumina (Al_2O_3) and silica (SiO_2) [8]. In the case of ZrO_2 addition, the flexural strength and fracture toughness of dense β-$Ca_3(PO_4)_2$ ceramics reach 199 MPa and 2.15 MPa $m^{1/2}$, respectively [6]. The flexural strength of β-$Ca_3(PO_4)_2$ ceramic also increases to 197 MPa by the addition of MgO; such increase is attributed to the partial stresses generated by the solid solution of magnesium ion into β-$Ca_3(PO_4)_2$ [7]. Moreover, the flexural strength of β-$Ca_3(PO_4)_2$ ceramic attains 271 MPa by the addition of Al_2O_3 and SiO_2 [8]. This noticeable enhancement of flexural strength is considered as (i) the promotion of densification due to the formation of liquid phases (∼ 1020 °C), (ii) the stabilization of β-phase, and (iii) restriction of the glassy phase formation in the presence of $AlPO_4$ [8].

Although various metal-oxides must also affect the densification of β-$Ca_3(PO_4)_2$ compact, no systematical information on the effect of metal-oxide addition on the sintering of β-$Ca_3(PO_4)_2$ has been available yet. The present authors reported the preparation conditions of high-purity β-$Ca_3(PO_4)_2$ powder by spray pyrolysis [9]. We further examined the sinterability of the resulting β-$Ca_3(PO_4)_2$ powder and found that the relative density of sintered β-$Ca_3(PO_4)_2$ compact attains 96.1% at a firing temperature as low as 1070 °C [10]. By making use of

*Author to whom all correspondence should be addressed.

such easily sinterable β-$Ca_3(PO_4)_2$ powder, we describe in this paper the effects of various metal-oxide additions on the sintering of β-$Ca_3(PO_4)_2$ powder.

2. Experimental procedures

2.1. Starting materials, compaction, and firing

The starting β-$Ca_3(PO_4)_2$ powder was prepared by the spray-pyrolysis of mixed solution with 0.9 mol dm^{-3} $Ca(NO_3)_2$ and 0.6 mol dm^{-3} $(NH_4)_2HPO_4$ at 600 °C, using an air–liquid nozzle. The spray-pyrolyzed powder was heated at 600 °C for 1 h and then was pulverized using a grinding apparatus (Model AGA, Ishikawa Kojo MFG). In this paper, either metal-oxide or metal-carbonate was used as an additive. The additives used in this paper were commercially available reagent grades: (i) monovalent metal-carbonates, Li_2CO_3, Na_2CO_3 and K_2CO_3; (ii) divalent metal-oxide and carbonates, MgO, $CaCO_3$, $SrCO_3$ and $BaCO_3$; (iii) trivalent metal-oxides, α-Al_2O_3 and Fe_2O_3; and (iv) tetravalent metal-oxides, SiO_2 (precipitated; non-crystalline powder), TiO_2 (anatase) and ZrO_2 (monoclinic). As shown above, some metal-carbonates were selected to take advantage of their high purities and chemical stabilities during the handling in air. These metal-carbonates ended up being converted into metal-oxides prior to the initiation of sintering.

The β-$Ca_3(PO_4)_2$ powder was mixed with the desired amount of metal-oxide or carbonate in the presence of acetone, using alumina mortar and pestle. Approximately 1.5 g of the mixture was uniaxially pressed at 30 MPa to form a cylindrical compact with a diameter of 20 mm and a thickness of around 2 mm. The compact was heated at the rate of 10 °C min^{-1} and was held at 1070 °C for 5 h in air.

2.2. Evaluation

The phase identification of sintered compact was conducted using an X-ray diffractometer (XRD; Model RAD-IIA, Rigaku; 40 kV, 25 mA) with Ni-filtered CuKα radiation and using a Fourier-transform infrared spectrometer (FT-IR; Model FT-IR8600PC, Shimadzu, Kyoto) with KBr method. The relative density of sintered compact was calculated by dividing the bulk density by the true density. The bulk density was measured on the basis of mass and dimensions, whereas the true density was measured picnometrically at 25.0 °C, using ethanol as replacement liquid. Fracture surfaces of the sintered compact were observed using a scanning electron microscope (SEM: Model S-4500, Hitachi, Tokyo; accelerating voltage, 10 kV).

3. Results and discussion

3.1. Monovalent metal-carbonate addition

The relative densities and crystalline phases of β-$Ca_3(PO_4)_2$ compacts with monovalent metal-oxide additions were examined by the pressureless sintering technique. Fig. 1 shows the effect of monovalent metal-oxide addition on the relative density of β-$Ca_3(PO_4)_2$ compact fired at 1070 °C for 5 h, together with typical SEM micrographs for fracture surfaces. The relative

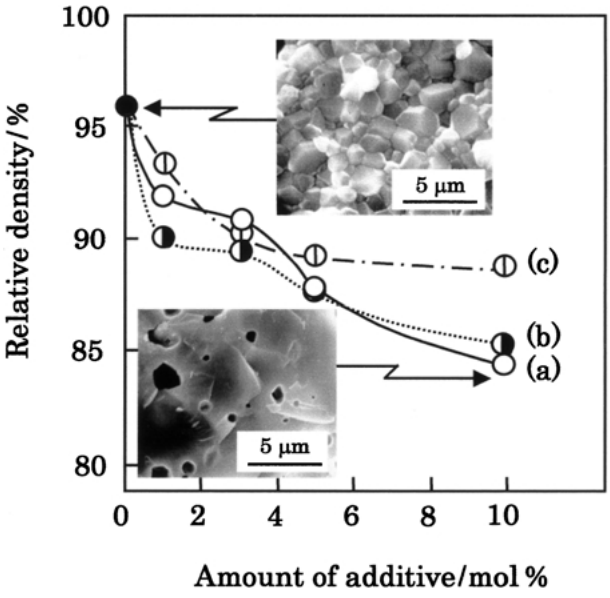

Figure 1 Effect of monovalent metal-oxide addition on the relative density of β-$Ca_3(PO_4)_2$ compact with (a) Li_2O addition, (b) Na_2O addition, and (c) K_2O addition fired at 1070 °C for 5 h, together with typical SEM micrographs for the fracture surfaces.

density of sintered β-$Ca_3(PO_4)_2$ compact decreased with increasing amount of monovalent metal-oxide addition. Relative densities of the sintered β-$Ca_3(PO_4)_2$ compacts with 10 mol % of monovalent metal-oxide additions were arranged as follows: K_2O addition > Na_2O addition > Li_2O addition. The SEM micrograph for the fracture surfaces of sintered β-$Ca_3(PO_4)_2$ compact without metal-oxide addition showed that the polyhedral grains with sizes of 1–3 μm were closely packed. On the other hand, SEM micrograph for the fracture surfaces of sintered β-$Ca_3(PO_4)_2$ compact with 10 mol % of Li_2O addition showed that the grain sizes were more than 5 μm, and that the spherical pores with diameters of 1–2 μm were present not only within grains but also on grain boundaries.

Comparing the microstructures of sintered β-$Ca_3(PO_4)_2$ compacts with and without Li_2O additions, we see that the grain growth and pore creation appear to be promoted by the addition of Li_2O. In order to make clear why such phenomena occurred due to the addition of Li_2O, the crystalline phases of sintered β-$Ca_3(PO_4)_2$ compacts with metal-oxide additions were examined using XRD and FT-IR. Typical XRD results for the sintered β-$Ca_3(PO_4)_2$ compacts with and without Li_2O additions are shown in Fig. 2. The sintered compact contained only β-$Ca_3(PO_4)_2$ [11] (Fig. 2(a)), whereas that with Li_2O addition contained not only β-$Ca_3(PO_4)_2$ but also HAp [12] (Fig. 2(b)). Although other XRD data were omitted in this paper, the sintered compacts with 10 mol % of Na_2O and K_2O additions also contained β-$Ca_3(PO_4)_2$ and HAp.

Since the sintered compacts with metal-oxide additions contained β-$Ca_3(PO_4)_2$ and HAp, FT-IR spectra for the pulverized powders were examined in order to check whether or not the OH group was present in the HAp structure. Typical FT-IR spectra for the β-$Ca_3(PO_4)_2$ powders with and without Li_2O additions are shown in Fig. 3. FT-IR spectrum for the pure β-$Ca_3(PO_4)_2$ powder showed that the absorption peaks appeared at 560, 600,

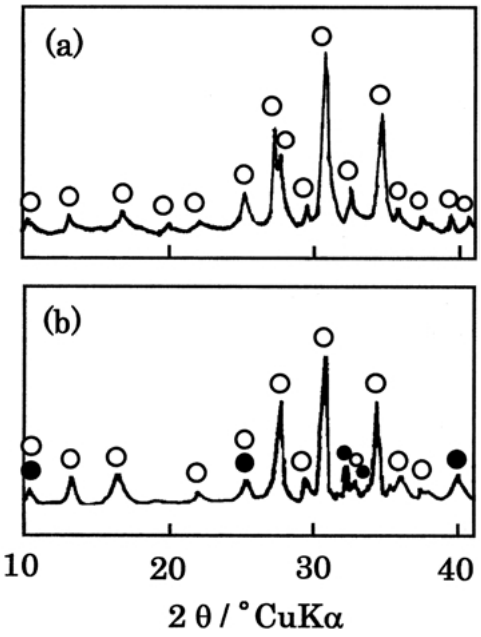

Figure 2 Typical XRD patterns for the (a) pure β-$Ca_3(PO_4)_2$ compact and (b) β-$Ca_3(PO_4)_2$ compact with 10 mol % of Li_2O addition fired at 1070 °C for 5 h. ○: β-$Ca_3(PO_4)_2$; ●: HAp.

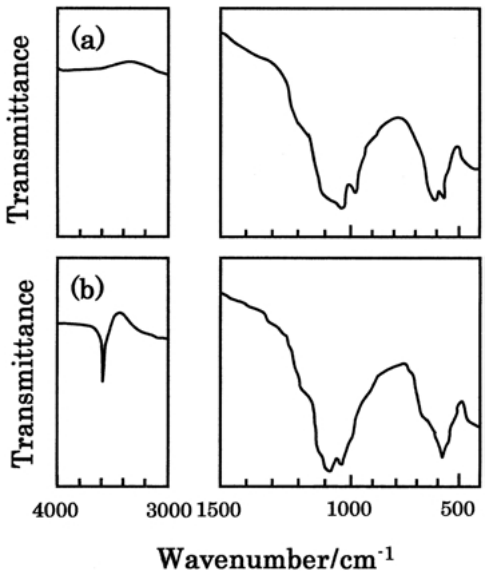

Figure 3 Typical FT-IR spectra for the (a) pure β-$Ca_3(PO_4)_2$ compact and (b) β-$Ca_3(PO_4)_2$ compact with 10 mol % of Li_2O addition fired at 1070 °C for 5 h.

970, and 1030 cm^{-1} (Fig. 3(a)). On the other hand, the FT-IR spectrum for the β-$Ca_3(PO_4)_2$ powder with 10 mol % of Li_2O addition showed absorption peaks at 590, 1030, 1090, and 3590 cm^{-1} (Fig. 3(b)).

The absorption peaks at 500–600, 970, and 1000–1100 cm^{-1} are assigned to the PO_4 group [13]. On the other hand, the peak at 3570 cm^{-1}, which appeared in the case of β-$Ca_3(PO_4)_2$ powder with 10 mol % of Li_2O addition, is assigned to the OH group [13]. The presence of OH group supports the XRD data that HAp was detected from the β-$Ca_3(PO_4)_2$ powder with 10 mol % of Li_2O addition.

The relative density of sintered β-$Ca_3(PO_4)_2$ compact decreases with increasing amount of monovalent metal-oxide addition. Although the sintered compacts with 10 mol % of monovalent metal-oxide additions contained not only β-$Ca_3(PO_4)_2$ but also HAp, the small amount of the metal-oxide (expressed as M^I) must show the solid solution into β-$Ca_3(PO_4)_2$ (chemical formula: $Ca_{3-x}M^I_{2x}(PO_4)_2$). With increasing amount of metal-oxide addition, the metal-oxide cannot continue the solid solution into β-$Ca_3(PO_4)_2$ any more but starts to react with β-$Ca_3(PO_4)_2$. The reaction of β-$Ca_3(PO_4)_2$ with 10 mol % of monovalent metal-oxide is, for example, expressed as follows:

$$0.9Ca_3(PO_4)_2 + 0.1M^I_2O \rightarrow Ca_{2.7}M^I_{0.2}(PO_4)_{1.8}O_{0.1} \quad (1)$$

The product, $Ca_{2.7}M^I_{0.2}(PO_4)_{1.8}O_{0.1}$, appears to react with moisture (H_2O) in the ambient atmosphere (air) to form HAp. As Equation 1 indicates, the solid-state reaction of β-$Ca_3(PO_4)_2$ with monovalent metal-oxide appears to be quite complex, but a small amount of metal ions must remain in the HAp structure.

According to the SEM micrographs, sizes of the β-$Ca_3(PO_4)_2$ grains with Li_2O addition are larger than those of pure β-$Ca_3(PO_4)_2$ grains. Such grain growth may be promoted by the presence of liquid phases formed during firing. Goto *et al*. [14] and Wakamatsu *et al*. [15] examined the densification behavior of HAp compact with Li_3PO_4 addition during firing. They found that (i) the grain growth is promoted by the formation of liquid phases in the β-$Ca_3(PO_4)_2$–Li_3PO_4 system at approximately 1010 °C and that (ii) the swelling of β-$Ca_3(PO_4)_2$ compact during firing is noted for the larger amount of Li_3PO_4 addition, chiefly due to the fusion and/or evaporation of reaction products. Our results on grain growth and pore creation may be related to such liquid-phase formation and the fusion/evaporation of reaction products, although the presence of Li_3PO_4 could not be confirmed by XRD. On the other hand, relative densities of the sintered β-$Ca_3(PO_4)_2$ compacts with 10 mol % of Na_2O and K_2O additions are slightly higher than the relative density of β-$Ca_3(PO_4)_2$ compact with 10 mol % of Li_2O addition. This fact may be explained by assuming that the swelling is restricted during firing, chiefly due to the limited amounts of fused and vaporized reaction products, compared to the case of Li_2O addition.

3.2. Divalent metal-oxide addition

Fig. 4 shows the effect of divalent metal-oxide addition on the relative density of β-$Ca_3(PO_4)_2$ compact fired at 1070 °C for 5 h, together with typical SEM micrographs for the fracture surfaces. Although the relative density of β-$Ca_3(PO_4)_2$ compact remained almost constant with increasing amount of MgO up to 4 mol %, it decreased with a further increase in the amount of MgO addition. On the other hand, the relative density of β-$Ca_3(PO_4)_2$ compact was reduced by the additions of CaO, SrO, and BaO. Relative densities of the β-$Ca_3(PO_4)_2$ compacts with divalent metal-oxide additions were arranged as follows: MgO addition > CaO addition > SrO addition > BaO addition. SEM micrographs for the fracture surfaces of sintered β-$Ca_3(PO_4)_2$ compacts with 10 mol % of MgO and BaO additions showed that the polyhedral grains with sizes of 1–2 μm were packed, but that the spherical pores with sizes of 0.5–1 μm and their linked pores were present on grain boundaries.

The crystalline phases of sintered compacts with

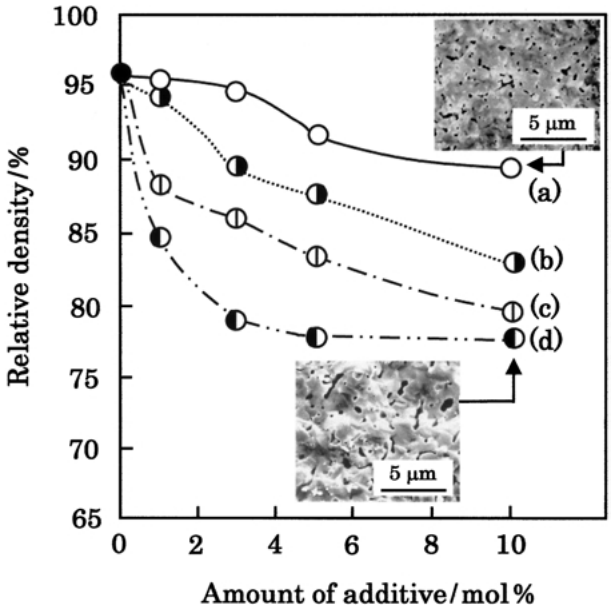

Figure 4 Effect of divalent metal-oxide addition on the relative density of β-$Ca_3(PO_4)_2$ compact with (a) MgO addition, (b) CaO addition, (c) SrO addition, and (d) BaO addition fired at 1070 °C for 5 h, together with typical SEM micrographs for the fracture surfaces.

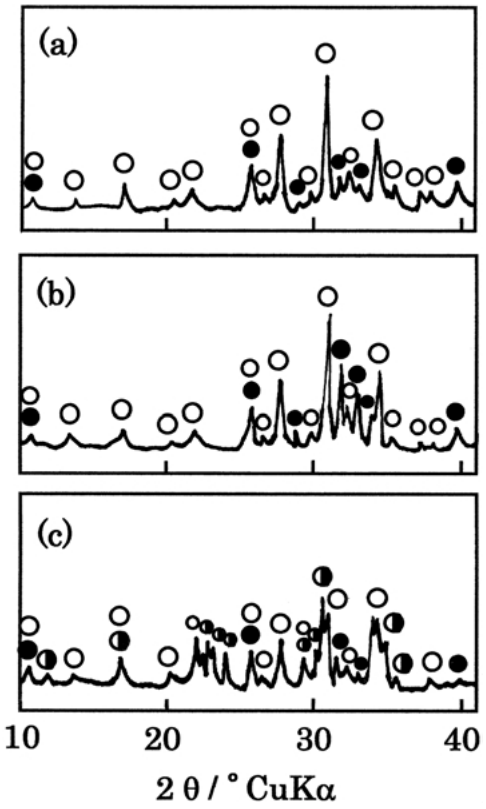

Figure 5 Typical XRD patterns for the β-$Ca_3(PO_4)_2$ compacts with 10 mol % of (a) MgO addition, (b) CaO addition, and (c) BaO addition fired at 1070 °C for 5 h. ◑: α-$Ca_3(PO_4)_2$; ○: β-$Ca_3(PO_4)_2$; ●: HAp.

divalent metal-oxide additions were checked using XRD. Typical results are shown in Fig. 5. The crystalline phases of sintered compacts with 10 mol % of MgO addition were β-$Ca_3(PO_4)_2$ and HAp (Fig. 5(a)). Although β-$Ca_3(PO_4)_2$ and HAp were also detected from the sintered compact with 10 mol % of CaO addition, the reflection intensities of HAp were much higher than those of sintered compact with MgO addition (Fig. 5(b)). The crystalline phases of sintered β-$Ca_3(PO_4)_2$ compact with 10 mol % of SrO addition were β-$Ca_3(PO_4)_2$ and HAp (XRD pattern was omitted in this paper). The crystalline phases of sintered β-$Ca_3(PO_4)_2$ compact with 10 mol % of BaO addition were α-$Ca_3(PO_4)_2$ [16], β-$Ca_3(PO_4)_2$, and HAp (Fig. 5(c)).

Referring to the effect of alkaline-earth oxide addition on the sintering of β-$Ca_3(PO_4)_2$, Toriyama *et al.* [7] reported as follows: (i) the solid solution may occur due to the substitution of 0.09–0.36 mass % (0.69–2.71 mol %) of MgO for Ca site in β-$Ca_3(PO_4)_2$ lattice; (ii) a part of the β-$Ca_3(PO_4)_2$ is thermally decomposed to form HAp when the amount of MgO addition increases to 0.72 mass % (5.3 mol %) or more; and (iii) the transformation temperature of β- to α-phase was lowered by the additions of SrO and BaO. Within the range of 4 mol % MgO addition, therefore, the mass transfer appears to be promoted by the solid solution of MgO into β-$Ca_3(PO_4)_2$. With a further increase in amount of MgO addition, however, the mass transfer is slowed down by the volume change, due to the formation of HAp in the presence of moisture in air.

The crystallinity of HAp is noted for the addition of CaO into β-$Ca_3(PO_4)_2$, which is related to an increase in Ca/P ratio. This enhanced crystallinity of HAp demonstrates that the divalent metal oxides, as well as monovalent metal oxides, may be incorporated into the HAp structure. On the assumption that 10 mol % of CaO participate in the formation of HAp, for example, the Ca/P ratio of the resulting HAp increases to 1.58. On the other hand, the relative density of β-$Ca_3(PO_4)_2$ compact was lowered by the additions of SrO and BaO additions, because SrO and BaO show little solid solution into β-$Ca_3(PO_4)_2$ but rather promote the reaction with β-$Ca_3(PO_4)_2$ to form HAp. Moreover, the transformation of β- to α-phase, as noted for the case of 10 mol % of BaO addition, must reduce the relative density or thermal expansion [7, 10].

3.3. Trivalent metal-oxide addition

Fig. 6 shows the effect of trivalent metal-oxide addition on the relative density of β-$Ca_3(PO_4)_2$ compact fired at 1070 °C for 5 h, together with typical SEM micrographs for the fracture surfaces. The relative density of β-$Ca_3(PO_4)_2$ compact decreased with increasing amount of Al_2O_3 addition. On the other hand, the relative density of β-$Ca_3(PO_4)_2$ compact increased with increasing amount of Fe_2O_3 and attained 98.7% at 10 mol % of Fe_2O_3 addition. SEM micrograph for the fracture surfaces of sintered β-$Ca_3(PO_4)_2$ compact with 10 mol % of Al_2O_3 addition showed that the corner-rounded grains with sizes of 1–2 μm were homogeneously packed, but that numerous pores were still present among grains. SEM micrographs for the fracture surfaces of sintered β-$Ca_3(PO_4)_2$ compact with 10 mol % of Fe_2O_3 addition showed that the polyhedral grains with sizes of approximately 2 μm were closely packed.

As shown above, there are marked differences in densification behavior and microstructural changes between Al_2O_3 and Fe_2O_3 additions. Since these phenomena are often caused by the crystalline phases present in the sintered compacts, crystalline phases of

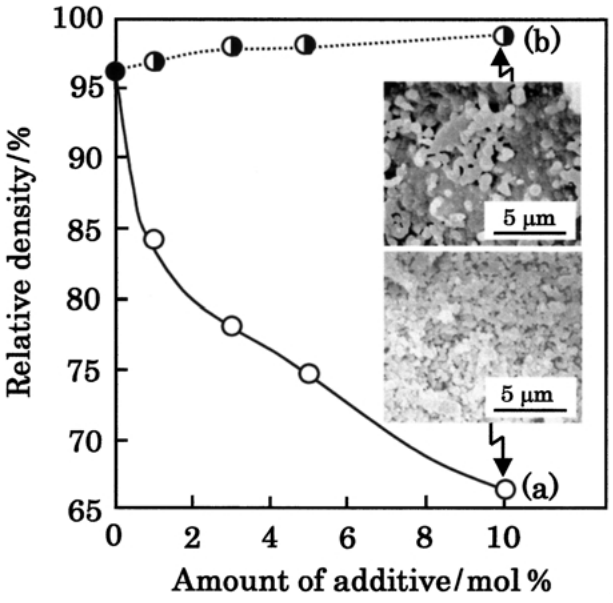

Figure 6 Effect of trivalent metal-oxide addition on the relative density of β-$Ca_3(PO_4)_2$ compact with (a) Al_2O_3 addition and (b) Fe_2O_3 addition fired at 1070 °C for 5 h, together with typical SEM micrographs for the fracture surfaces.

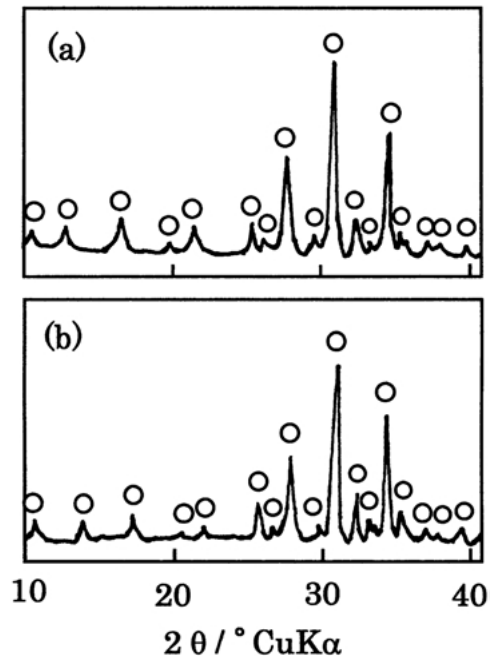

Figure 7 Typical XRD patterns for the β-$Ca_3(PO_4)_2$ compacts with 10 mol % of (a) Al_2O_3 addition and (b) Fe_2O_3 addition fired at 1070 °C for 5 h. ○: β-$Ca_3(PO_4)_2$.

these sintered β-$Ca_3(PO_4)_2$ compacts with Al_2O_3 and Fe_2O_3 additions are examined using XRD. Results are shown in Fig. 7. The crystalline phase of sintered compacts with Al_2O_3 and Fe_2O_3 additions was only β-$Ca_3(PO_4)_2$ (Fig. 7(a) and (b)).

Among these trivalent metal-oxide additions, Toriyama *et al*. [8] pointed out that β-phase is not stabilized by the addition of Al_2O_3 and that the bulk density of sintered β-$Ca_3(PO_4)_2$ compact is reduced by the addition of Al_2O_3. Although reaction products could not be detected from the present sintered β-$Ca_3(PO_4)_2$ compact with Al_2O_3 addition, they must be present as secondary phases on grain boundaries and appear to restrict the mass transfer. Actually, Ji and Marquis [17] reported that the calcium aluminates, which are formed by the sintering of HAp with Al_2O_3 addition, restrict the densification.

On the other hand, our previous data on the lattice parameters of β-$Ca_3(PO_4)_2$ with Fe_2O_3 addition [18] are almost in accord with those of the pure β-$Ca_3(PO_4)_2$ ($a \simeq 1.043$ and $c \simeq 3.738$ nm) [19], demonstrating that no marked solid solution of Fe_2O_3 into β-$Ca_3(PO_4)_2$ occurs during the firing at 1070 °C. Previously, Ando [5] reported that Fe_2O_3 may form the solid solution with β-$Ca_3(PO_4)_2$, but that the effect is not so remarkable, compared to the case of MgO addition. The densification of β-$Ca_3(PO_4)_2$ compact with Fe_2O_3 addition appears to be promoted by the formation of liquid phase. According to the phase diagram in the Fe_2O_3–P_2O_5 system, the liquid phase(s) in the $2Fe_2O_3 \cdot P_2O_5$-$Fe_2O_3 \cdot P_2O_5$ system and/or $Fe_2O_3 \cdot P_2O_5$-$2Fe_2O_3 \cdot 3P_2O_5$ system may form above 950 °C [20]. The liquid phases help the rearrangement of grains toward closer packing, thereby promoting the densification.

3.4. Tetravalent metal-oxide addition

Fig. 8 shows the effect of tetravalent metal-oxide addition on the relative density of β-$Ca_3(PO_4)_2$ compact fired at 1070 °C for 5 h, together with typical SEM micrographs for the fracture surfaces. Relative densities of the β-$Ca_3(PO_4)_2$ compacts slightly decreased with increasing amounts of SiO_2 and ZrO_2 additions. However, no appreciable changes in the relative density of β-$Ca_3(PO_4)_2$ compact were observed with increasing amount of TiO_2 addition. The SEM micrograph for the fracture surfaces of sintered β-$Ca_3(PO_4)_2$ compact with 10 mol % of TiO_2 addition showed that the polyhedral grains with sizes of 1–2 μm were closely packed. The SEM micrograph for the fracture surfaces of sintered β-$Ca_3(PO_4)_2$ compact with 10 mol % of SiO_2 addition

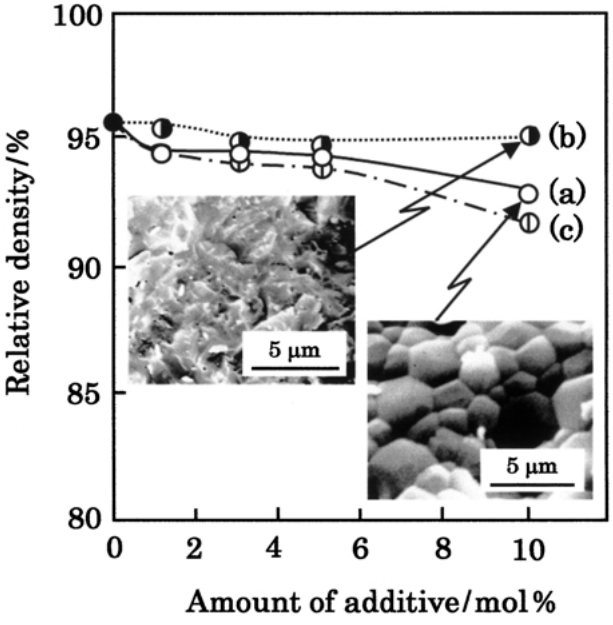

Figure 8 Effect of tetravalent metal-oxide addition on the relative density of β-$Ca_3(PO_4)_2$ compact with (a) SiO_2 addition, (b) TiO_2 addition, and (c) ZrO_2 addition fired at 1070 °C for 5 h, together with typical SEM micrographs for the fracture surfaces.

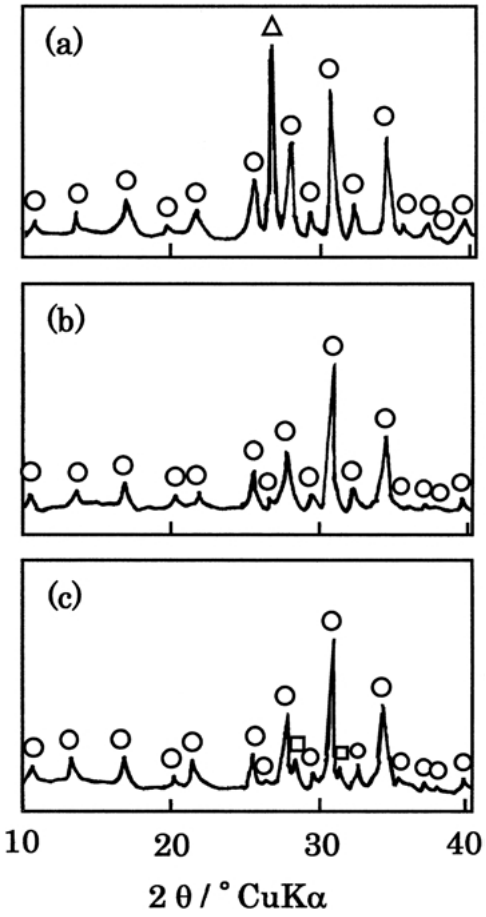

Figure 9 Typical XRD patterns for the β-$Ca_3(PO_4)_2$ compacts with 10 mol % of (a) SiO_2 addition, (b) TiO_2 addition, and (c) ZrO_2 addition fired at 1070 °C for 5 h. ○: β-$Ca_3(PO_4)_2$ △: SiO_2 (α-quartz) □: ZrO_2 (monoclinic).

showed that the polyhedral grains with diameters of 1–5 μm were present.

The crystalline phases of sintered compacts with tetravalent metal-oxide additions are shown in Fig. 9. The crystalline phases of sintered compact with SiO_2 addition were β-$Ca_3(PO_4)_2$ and SiO_2 (α-quartz) [21] (Fig. 9(a)). The crystalline phase of sintered compact with TiO_2 addition was only β-$Ca_3(PO_4)_2$ (Fig. 10(b)). Moreover, the crystalline phases of sintered compact with ZrO_2 addition were β-$Ca_3(PO_4)_2$ and ZrO_2 (monoclinic) [22] (Fig. 9(c)).

The densification of β-$Ca_3(PO_4)_2$ compact with metal-oxide addition must be proceeded by the solid solution and/or by the formation of liquid phases. These cation radii are as follows: Si^{4+}, 0.041 nm; Ti^{4+}, 0.068 nm; and Zr^{4+}, 0.080 nm [23]. Since the cation radius of Ti^{4+} is 0.068 nm, which is close to Mg^{2+} radius of 0.065 nm, a part of Ti^{4+} may show solid solution into β-$Ca_3(PO_4)_2$ lattice [24]. On the other hand, Si^{4+} and Zr^{4+} show little solid solution into β-$Ca_3(PO_4)_2$ during the firing. In fact, neither SiO_2 [8] nor ZrO_2 addition [6] contributes to restricting the transfomation from β- to α-phase.

3.5. Overall view of the effect of metal-oxide addition

In Sections 3.1–3.4, we described the effect of metal-oxide addition on the sintering of β-$Ca_3(PO_4)_2$ compact. As we mentioned before, the previous researchers have paid much attention to the metal-oxide addition from the viewpoints of not only the densification process and mechanical properties but also the stabilization of β-phase. Based upon these aspects, the present data are summarized, together with the previous data on the phase transformation by the metal-oxide additions. Results are shown in Table I. Note that the crystalline phases and relative densities are listed for the case of 10 mol % of metal-oxide addition. According to the previous reports, β-phase may be stabilized when the metal ions show solid solution into $Ca_3(PO_4)_2$. The stabilization of β-phase is advantageous to the sintering, partly because the β-$Ca_3(PO_4)_2$ compact can be fired at comparatively higher temperatures, and partly because the formation of solid solution restricts the grain growth to help in eliminating the residual pores along grain boundaries. Relative densities of the sintered $Ca_3(PO_4)_2$ compacts were reduced by the additions of metal-oxides, except for the case of Fe_2O_3 addition, which indicates that the secondary phases present on and near grain boundaries restrict the mass transfer across the grain boundaries. Nevertheless, the stabilization of β-phase enables fabrication of dense β-$Ca_3(PO_4)_2$ ceramics, because the β-$Ca_3(PO_4)_2$ compact may be fired above the transformation temperature of β-$Ca_3(PO_4)_2$ (1120–1180 °C [25]). Actually, other researchers [6] reported that the β-$Ca_3(PO_4)_2$ compact with 6 mol % of Y_2O_3 addition is

TABLE I Overall view of the present results, together with the data on stabilization of β-phase reported by previous researchers

Valence	Additive	C.R.[a] (nm)	Crystalline phase	R.D.[b] (%)	Stabilization of β-phase[c]
I	Li_2O	0.060	β-$Ca_3(PO_4)_2$, HAp	84.7	
	Na_2O	0.095	β-$Ca_3(PO_4)_2$, HAp	85.3	+[d]
	K_2O	0.133	β-$Ca_3(PO_4)_2$, HAp	89.7	
II	MgO	0.065	β-$Ca_3(PO_4)_2$, HAp	89.6	+[d,e]
	CaO	0.099	β-$Ca_3(PO_4)_2$, HAp	82.9	
	SrO	0.113	β-$Ca_3(PO_4)_2$, HAp	79.7	−[e]
	BaO	0.135	β-$Ca_3(PO_4)_2$, HAp	78.0	−[d,e]
III	$A1_2O_3$	0.050	β-$Ca_3(PO_4)_2$	66.3	±[f]
	Fe_2O_3	0.064	β-$Ca_3(PO_4)_2$	98.7	+[d]
IV	SiO_2	0.041	β-$Ca_3(PO_4)_2$, SiO_2	93.2	±[f]
	TiO_2	0.068	β-$Ca_3(PO_4)_2$	95.3	±[g]
	ZrO_2	0.080	β-$Ca_3(PO_4)_2$, ZrO_2	92.1	±[h]

[a] Cation radius. [b] Relative density, 10 mol % addition. [c] +: Positive effect, ±: No marked effect, −: Negative effect. [d] Ref. (5). [e] Ref. (7). [f] Ref. (8). [g] Ref. (24). [h] Ref. (6).

fired at temperature as high as 1400 °C and that the average bending strength attains 199 MPa, compared to the case of pure β-$Ca_3(PO_4)_2$ (138 MPa).

4. Conclusion

The effect of metal-oxide addition on the sintering of β-$Ca_3(PO_4)_2$ was examined. The metal-oxides used were as follows: (i) monovalent metal oxides, Li_2O, Na_2O, and K_2O; (ii) divalent metal oxides, MgO, CaO, BaO, and SrO; trivalent metal oxides, Al_2O_3 and Fe_2O_3; and (iv) tetravalent metal oxides, SiO_2, TiO_2, and ZrO_2. The results obtained can be summarized as follows:

1. The relative density of sintered β-$Ca_3(PO_4)_2$ compact was reduced with increasing amount of monovalent metal-oxide addition. The sintered compacts contained not only β-$Ca_3(PO_4)_2$ but also HAp.

2. The relative density of sintered β-$Ca_3(PO_4)_2$ compact was reduced with increasing amount of divalent metal-oxide addition, except for the case in which the relative density of sintered β-$Ca_3(PO_4)_2$ compact with MgO addition remained constant with increasing amount of MgO up to 4 mol %. Although the sintered compacts with MgO, CaO, and SrO additions contained β-$Ca_3(PO_4)_2$ and HAp, the sintered compact with BaO addition included α-$Ca_3(PO_4)_2$, β-$Ca_3(PO_4)_2$, and HAp.

3. In the case of trivalent metal oxide additions, the relative density of sintered β-$Ca_3(PO_4)_2$ compact was reduced with increasing amount of Al_2O_3 addition, whereas it was enhanced with increasing amount of Fe_2O_3 addition and reached 98.7% at 10 mol % Fe_2O_3 addition. In both cases, no crystalline reaction products were detected from the sintered compacts.

4. In the case of tetravalent metal-oxide additions, relative densities of the sintered β-$Ca_3(PO_4)_2$ compacts were slightly reduced with increasing amounts of SiO_2 and ZrO_2 additions, whereas no appreciable changes in the relative density were observed with increasing amount of TiO_2 addition. The sintered compacts with SiO_2 and ZrO_2 additions included SiO_2 (α-quartz) and ZrO_2 (monoclinic), respectively, together with β-$Ca_3(PO_4)_2$.

References

1. M. JARCHO, R. L. SALSBURY, M. B. THOMAS and R. H. DOREMUS, *J. Mater. Sci.* **14** (1979) 142.
2. L. L. HENCH, *J. Am. Ceram. Soc.* **81** (1998) 1705.
3. D. S. METGER, M. R. RIEGER and D. W. FOREMAN, *J. Mater. Soc.* **10** (1999) 9.
4. M. AKAO, H. AOKI, K. KATO and A. SATO, *J. Mater. Sci.* **17** (1982) 343.
5. J. ANDO, *Bull. Chem. Soc. Jpn* **31** (1958) 196.
6. M. AKAO, H. AOKI, K. TACHIMOTO and T. YAMAMOTO, *Yogyo-Kyokai-Shi* **95** (1987) 819.
7. M. TORIYAMA, S. KAWAMURA, H. NAGASE and K. ISHIDA, *ibid.* **95** (1987) 822.
8. M. TORIYAMA, S. KAWAMURA, Y. ITO, H. NAGASE and I. TOYAMA, *J. Ceram. Soc. Jpn* **96** (1988) 837.
9. K. ITATANI, M. AIZAWA, F. S. HOWELL, A. KISHIOKA and M. KINOSHITA, *Phosphorus Res. Bull.* **1** (1991) 35.
10. K. ITATANI, T. NISHIOKA, S. SEIKE, F. S. HOWELL, A. KISHIOKA and M. KINOSHITA, *J. Am. Ceram. Soc.* **77** (1994) 801.
11. Powder Diffraction File Card No. 9-169 (JCPDS International Center for Diffraction Data, Newton Square, PA).
12. Powder Diffraction File Card No. 24-33 (JCPDS International Center for Diffraction Data, Newton Square, PA).
13. R. R. RAO, H. N. ROOPA and T. S. KANNAN, *J. Mater. Sci.: Mater. Med.* **8** (1997) 511.
14. T. GOTO, N. WAKAMATSU, H. KAMEMIZU, M. IIJIMA, Y. DOI and Y. MORIWAKI, *ibid.* **2** (1991) 149.
15. N. WAKAMATSU, T. GOTO, H. KAMEMIZU, M. IIJIMA, Y. TAKEZAWA, H. MIZUGUCHI, S. IMURA, K. HAYASHI, S. SHIBATA, Y. DOI and Y. MORIWAKI, *Yogyo-Kyokai-Shi* **95** (1987) 831.
16. Powder Diffraction File Card No. 29-359 (JCPDS International Center for Diffraction Data, Newton Square, PA).
17. H. JI and P. M. MARQUIS, *J. Mater. Sci.* **28** (1993) 1941.
18. K. ITATANI, M. TATAKASHI, M. AIZAWA, F. S. HOWELL and A. KISHIOKA, *Phosphorus Res. Bull.* **6** (1996) 171.
19. B. DICKENS, L. W. SHROEDER and W. E. BROWN, *J. Solid State Chem.* **10** (1974) 232.
20. H. WENTRUP, *Arch. Eisenhüettenw.* **9** (1935–36) 57.
21. Powder Diffraction File Card No. 5-490 (JCPDS International Center for Diffraction Data, Newton Square, PA).
22. Powder Diffraction File Card No. 36-420 (JCPDS International Center for Diffraction Data, Newton Square, PA).
23. M. C. DAY, JR. and J. SELBIN, in ''Theoretical Inorganic Chemistry'' (Reinhold Publishing, New York, 1962) p. 96.
24. K. ITATANI, M. AIZAWA, A. KISHIOKA and M. KINOSHITA, *Gypsum & Lime*, No. 238 (1992) 168.
25. H. MONMA and M. GOTO, *Yogyo-Kyokai-Shi* **91** (1983) 473.

Received 10 April
and accepted 7 September 2001